Flexible ZnO transparent thin-film transistors by a solution-based process at various solution concentrations

Flexible ZnO transparent thin-film transistors by a solution-based process at various solution concentrations

C Y Lee[1]**, M Y Lin**[1]**, W H Wu**[1]**, J Y Wang**[2]**, Y Chou**[3]**, W F Su**[3]**, Y F Chen**[2]
and C F Lin[1,4]

[1] Graduate Institute of Photonics and Optoelectronics, National Taiwan University, Taipei 10617,
Taiwan, Republic of China
[2] Department of Physics, National Taiwan University, Taipei 10617, Taiwan, Republic of China
[3] Department of Materials Science and Engineering, Graduate Institute of Materials Science and
Engineering, National Taiwan University, Taipei 10617, Taiwan, Republic of China
[4] Department of Electrical Engineering, Graduate Institute of Electronics Engineering, National Taiwan
University, Taipei 10617, Taiwan, Republic of China

E-mail: cflin@cc.ee.ntu.edu.tw

Abstract
We report solution-processed ZnO thin-film transistors (TFTs) on a flexible substrate, using
polymethylmethacrylate (PMMA) as a dielectric layer. To improve the compatibility between
the ZnO active layer and the PMMA dielectric, an O_2-plasma treatment has been applied to the
PMMA dielectric. The structural and electrical characteristics of the ZnO-TFTs, which have
different channel morphologies produced by various concentrations of the ZnO solution, were
investigated. The ZnO trap centers of the ZnO-TFTs were decreased as the concentration of
the ZnO solution increased. The ZnO-TFT with the optimized channel morphology exhibited
a high field-effect mobility of 7.53 cm^2 V^{-1} s^{-1}.

(Some figures in this article are in colour only in the electronic version)

Currently, transparent electronics based on a flexible substrate are one of the most crucial technologies for the next generation of optoelectronic devices, such as displays, home electronic appliances and photovoltaics [1, 2]. Hence, transparent thin-film transistors (TFTs) on flexible substrates are key devices for realizing these transparent electronic products. Although an organic TFT and its manufacturing process are suitable for flexible substrates [3, 4], their low mobility and extreme sensitivities to oxygen and moisture overshadow their device performance attributes. TFTs that use ZnO have the advantages of high charge mobility, excellent environmental stability and high transparency in comparison to TFTs that are based on organic semiconductors [5, 6].

ZnO can be deposited through various methods, such as molecular beam epitaxy, pulsed laser deposition and chemical vapor deposition [7, 8]. However, these methods are not compatible with flexible TFT manufacturing because a high processing temperature or an additional annealing process is required to obtain good transistor properties [9–11]. Although a few studies have examined the fabrication of flexible ZnO-TFTs through the solution process at relatively low temperatures, the devices show a distinctly lower mobility because of high trap centers in a ZnO active layer [12, 13]. Here, we utilized organic–inorganic heterostructure to prepare high-performance ZnO-TFTs on a flexible substrate with low-temperature processes (<150 °C). In order to reduce the trap centers, the morphology of the ZnO active layer was controlled by changing the concentration of the ZnO solution. The optimized device shows a high mobility of 7.53 cm^2 V^{-1} s^{-1} and an excellent current on–off ratio of more than 10^4. The processing procedure that is revealed in this work shows a convenient and low-cost method for fabricating flexible ZnO-TFTs.
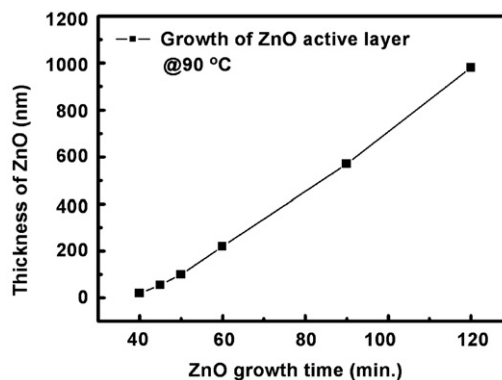
A schematic diagram of the ZnO-TFT is shown in figure 1(*a*). We adopted the top-contact geometry; the channel width (*W*) and length (*L*) were 100 and 20 μm,
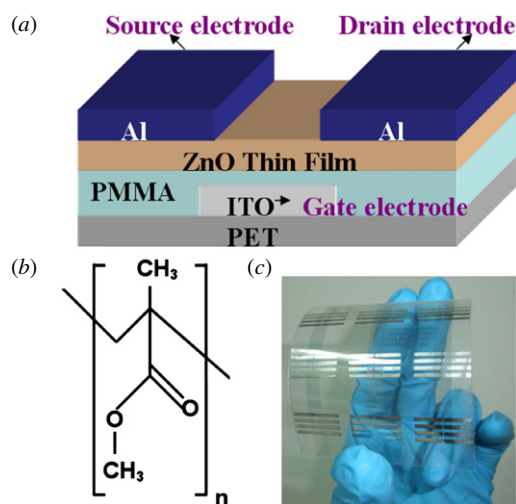
Figure 1. (*a*) Schematic illustration of the ZnO-TFT device structure. (*b*) The chemical structure of PMMA. (*c*) Photograph of the ZnO-TFT.

Figure 2. Effect of the growth time on the thickness of the ZnO active layer.

respectively. The devices were fabricated on transparent indium tin oxide (ITO)-coated polyethylene terephthalate (PET, 175 μm) substrates. First, the PMMA powder was dissolved in toluene with a concentration of 8 wt%; next, it was spin-coated onto the ITO-PET substrate to form a 200 nm thick polymer dielectric. The sample was then annealed at 120 °C for 2 h to remove the residual solvent, to ensure good contacts between the ITO-PET substrate and the PMMA layer. The molecular structure of PMMA is shown in figure 1(*b*). To enhance compatibility at the interface between the PMMA dielectric and the ZnO active layer, the PMMA dielectric was O_2-plasma-treated with an rf power of 20 W for 10 s. When PMMA was treated with O_2 plasma, the chains on the surface were broken, and polar and hydrophilic functional groups such as $-OH$ and $-COOH$ were introduced, resulting in an increase of the surface energy [14]. Since the increased surface energy of the PMMA dielectric ensures a sufficient wetting of the ZnO seeding layer on the dielectric surface, the coverage of the ZnO seeding layer on the PMMA surface was improved [13].

The ZnO active layer was synthesized on a PMMA dielectric via a hydrothermal process. To facilitate the nucleation of ZnO layer growth, 500 mM of a 1:1 molar solution of zinc acetate dihydrate (Sigma-Aldrich, 99.999% purity) and monoethanolamine (Sigma-Aldrich, 99.5% purity) in isopropyl alcohol was spin-coated onto the plasma-treated PMMA dielectric to form a ZnO seeding layer [15]. Afterwards, the seeding layer was annealed at 100 °C for 1 h to remove the residual solvent. The hydrothermal growth of the ZnO active layer was achieved by suspending the seeded substrate upside down in a ZnO aqueous solution at 90 °C for 50 min. The ZnO solution containing zinc nitrate ($Zn(NO_3)_2 \cdot 6H_2O$, Sigma-Aldrich, 98% purity) and equivalent molar hexamethylenetetramine ($C_6H_{12}N_4$, Sigma-Aldrich, 99.5% purity) dissolved in deionized water [16]. In our growth system, the ZnO aqueous solution is heated from room temperature to 90 °C at a rate of 1.56 °C min^{-1} during the hydrothermal process. The growth rate of the ZnO active layer increases as a function of the growth temperature. In general the average growth rates of the ZnO active layer for the growth temperatures of <90 °C and 90 °C are 1.22 nm min^{-1} and 12.6 nm min^{-1}, respectively. The ZnO growth thickness versus growth time plot of the ZnO/PMMA sample is shown in figure 2.

For this work, three concentrations of the ZnO aqueous solution (110, 80 and 50 mM) were used for comparison. After the ZnO active layer was deposited, the samples were baked at 100 °C for 2 h. Finally, source/drain electrodes were defined on the ZnO active layer by thermally evaporating 200 nm thick aluminum to form a continuous coating. A photograph of the flexible ZnO-TFTs, as described here, is shown in figure 1(*c*). The capacitance of the dielectric was measured with an HP 4284A precision LCR meter. The capacitance per unit area (C_i) of the plasma-treated PMMA dielectric was found to be 8.6 nF cm^{-2}.

All the optical transmittance of the deposited films was measured using a UV–visible scanning spectrophotometer (Lambda 35) at wavelengths from 350 to 900 nm, as shown in figure 3. Curve (a) shows the transmittance spectrum through the ZnO-TFT, which includes the ITO-PET substrate, PMMA dielectric and the ZnO film. The ZnO-TFT is transparent in the visible range of 400–800 nm, with a transmittance range from 65% to approximately 93%. To understand the contribution of each film to the optical characteristics, the corresponding transmittance spectrum is also measured. Curve (b) represents the transmittance spectrum of the ITO-PET substrate (black line). It shows the transmittance of about 78–95% in the range from 400 to 800 nm, indicating a good transmittance of visible light. Ripples in curve are caused by absorption of the PET substrate. Curves (c) and (d) show the transmittance spectra of the PMMA dielectric (red line) and the ZnO film (green line), respectively, with the substrate absorption removed. These films show average optical transmissions of >90%. It indicates that the transmission losses due to these films are negligible and visible light can readily penetrate the ZnO/PMMA heterostructure.

As displayed in the inset of figure 3, our ZnO active layer on the PMMA/ITO-PET substrate at a deposition concentration of 110 mM has a dense structure with compact
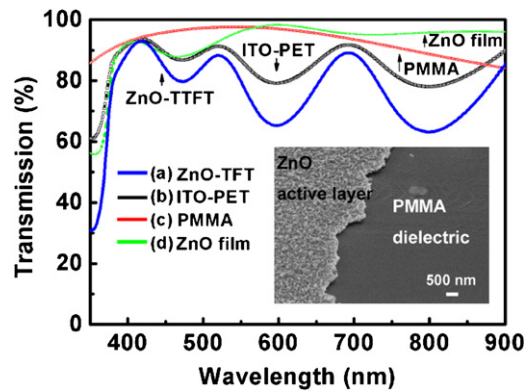
Figure 3. Optical transmittance spectra for the ZnO-TFT through the ITO-PET substrate, PMMA and the ZnO active layer. The inset shows the FESEM image of the ZnO active layer on the PMMA dielectric.


Figure 4. (*a*) TEM image of the ZnO/PMMA thin film on a glass substrate. (*b*) High-resolution TEM image of the ZnO NR. The inset shows the selected area electron diffraction image from one individual ZnO NR.

amassment grains, as revealed by field-emission scanning electron microscopy (FESEM, LEO 1530). In order to provide sufficient device isolation, we set the distance between the adjacent TFTs to greater than 1 mm to reduce the interference current. The interference current decreases as the spacing between the first and second TFTs increases because the channel has a finite resistance. The size of each device is determined by patterned deposition of source/drain electrodes.

The morphology of ZnO/PMMA was examined using transmission electron microscopy (TEM, Philips Tecnai F30). In order to prepare the TEM sample, we deposited the ZnO/PMMA thin film on a glass substrate. Here, the ZnO active layer was deposited at a ZnO deposition concentration of 110 mM for 2 h. Figure 4(*a*) shows the cross-sectional TEM image of the ZnO/PMMA thin film, which indicates that through the hydrothermal method, a ZnO active layer can be compactly grown on the PMMA dielectric. The ZnO active layer consists of many ZnO nanorods (NRs), implying that the grain boundaries as electron scattering centers could be decreased with increasing grain size. Therefore, it is expected that the electron mobility would increase due to the lower scattering centers, as the diameter of the ZnO NR increases. The high-resolution TEM (HRTEM) image of lattice fringes, taken from the head of a NR displayed in figure 4(*a*), is shown in figure 4(*b*), which presents an atomic-resolved single crystal wurtzite lattice structure along the [0 0 0 1] growth direction of the *c*-axis [17]. The edge of the NR is clear, and no amorphous layer is observed on the surface. The inset shows the selected area electron diffraction pattern from a NR, which also indicates that the NR is single-crystal ZnO with wurtzite structure. This indicates that through the hydrothermal method, ZnO grains can be grown on the PMMA layer with good crystalline quality.

In order to investigate the effects of grain boundaries on the flexible ZnO-TFTs, we studied ZnO-TFTs that had three kinds of ZnO channel morphologies, which grew for 50 min at the ZnO solution concentrations of 110, 80 and 50 mM, respectively. The ZnO morphologies of the devices have been characterized by FESEM, as shown in the insets of figures 5(*a*), (*c*) and (*e*). The FESEM images show that the grain sizes of
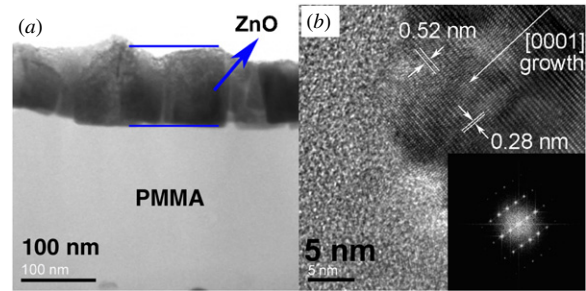
ZnO were very different. The grain size increased from 75 to 175 nm when the ZnO solution concentration increased from 50 to 110 mM. In addition, all the resulting ZnO layers had the same thickness of about 100 nm, as measured by a surface profiler (*Alpha*-Step 500). This demonstrates that the ZnO solution concentrations can significantly affect the grain size of the ZnO active layer, not the thickness of ZnO.

Figures 5(*a*)–(*f*) show the output and transfer characteristics for ZnO-TFTs grown at the ZnO solution concentrations of 110, 80 and 50 mM. We measured the electrical characteristics of individual transistors using a probe station for making electrical contact with devices and an HP 4156C parameter analyzer for the measurements. The field effect mobility (μ) and threshold voltage (V_T) values were calculated from the slope of the plot of the square root of the drain–source current (I_{DS}) versus the gate voltage (V_G) in the regime of the drain–source voltage (V_{DS}) = 20 V, using the equation $I_{DS} = (WC_i/2L)\mu(V_G-V_T)^2$. The different ZnO grown concentrations produced a range of ZnO-TFT properties, even though the thicknesses of the ZnO active layers were the same. Additionally, the ZnO-TFTs built on the ZnO seeding layer without the ZnO NR film showed no TFT behavior (not shown here). These findings also reveal that the TFT characteristics presented in figures 5(*a*)–(*f*) resulted from the ZnO NR film, not the ZnO seeding layer. In other words, the ZnO-TFT properties are strongly dependent on the channel of the ZnO NR film. The mobility was highest at 7.53 cm^2 V^{-1} s^{-1} for the 110 mM preparation and lowest at 0.097 cm^2 V^{-1} s^{-1} for the 50 mM preparation, with 0.69 cm^2 V^{-1} s^{-1} for the 80 mM preparation.

Furthermore, the device grown in the 110 mM ZnO solution exhibited the highest current on–off ratio, more than 10^4, and the lowest threshold voltage, 5.4 V. In contrast, the device grown at a lower concentration, in the 50 mM ZnO solution (which resulted in a ZnO active layer with higher filling of the NRs, more grain boundaries and more trap centers), showed a markedly lower current on–off ratio of $\sim$10^2 and a higher threshold voltage of 14.5 V. As a result, no saturation behavior was observed in the TFT shown in figure 5(*e*). We consider that a highly uniform and densely packed array of large grain sizes of ZnO NRs, produced by a higher concentration of the ZnO solution, reduced the number of the trap centers, leading to an improvement in the carrier mobility, current on-off ratio and threshold voltage.
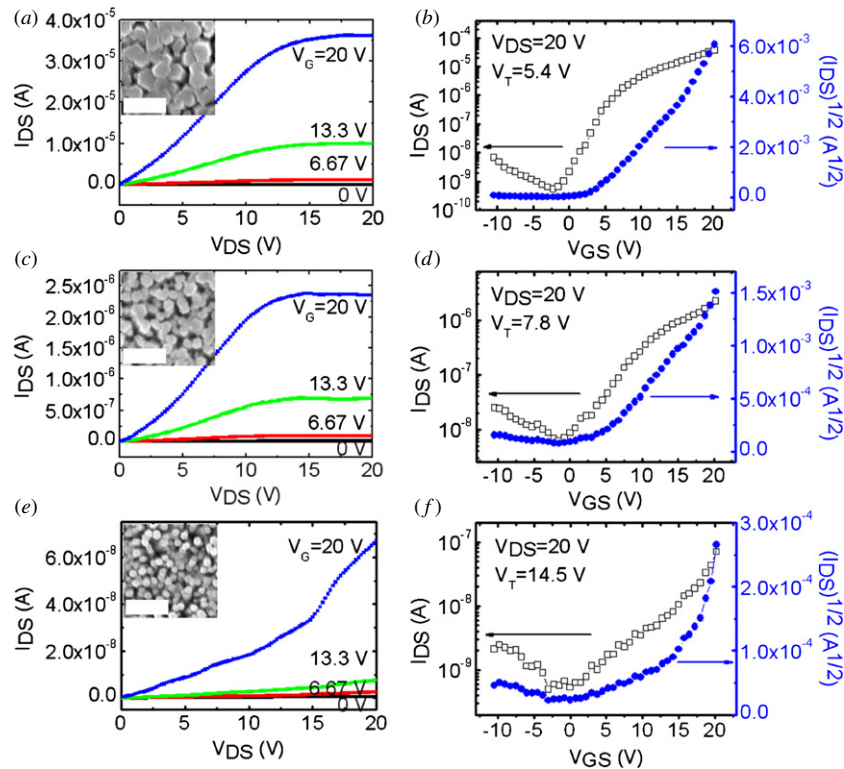
Figure 5. Transistor output curves for ZnO-TFTs, fabricated with the ZnO solution concentration at (*a*) 110 mM, (*c*) 80 mM and (*e*) 50 mM. The corresponding transistor transfer characteristics are (*b*) 110 mM, (*d*) 80 mM and (*f*) 50 mM. The inset shows the corresponding FESEM images. The scale bar is 500 nm.

Additionally, the output curves in figures 5(*a*), (*c*) and (*e*) all show nonlinear behavior near $V_{DS} = 0$. We attribute the nonlinear behavior to nonlinear source/drain contact resistance. The nonlinear source/drain contact resistance is due to Schottky-barrier tunneling between the ZnO active layer and the electrode at increased gate bias voltages. The characteristics of such contacts result in the contact resistance of the device being both gate-voltage and drain-voltage dependent [18]. Hence, for the device with Schottky contacts, the slope in the triode region is convex until becoming concave just before saturation.

Although we have demonstrated an impressive improvement in the field effect mobility over previously reported flexible ZnO-TFTs, the sub-threshold slopes (S) are rather poor, even the best device still has $S > 2$ V/dec. This means that the PMMA/ZnO interface is still not optimized. Considering that, we will have to use a more stable dielectric material to match the ZnO active layer in the future, it could be expected that better device performance will be gained.

In conclusion, we have fabricated a transparent ZnO-TFT by a hydrothermal method using a polymeric PMMA film as the gate insulating film. An O_2-plasma treatment was applied to the PMMA dielectric to enhance compatibility between the ZnO active layer and the PMMA dielectric at the interface. Moreover, the effect of the ZnO morphology on the TFT properties has been investigated. The optimized ZnO-TFT shows a good saturation mobility of 7.53 cm^2 V^{-1} s^{-1} and a drain current on-to-off ratio of more than 10^4. This research

implies that a ZnO-TFT produced on a flexible substrate by a low-cost, simple technique could be applicable to the next generation of optoelectronics.

References

[1] Ju S, Facchetti A, Xuan Y, Liu J, Ishikawa F, Ye P, Zhou C, Marks T J and Janes D B 2007 *Nat. Nanotechnol.* **2** 378–84
[2] Kim S, Ju S, Back J H, Xuan Y, Ye P D, Shim M, Janes D B and Mohammadi S 2008 *Adv. Mater.* **20** 1–5
[3] Lee K H, Lee G, Lee K, Oh M S and Im S 2009 *Appl. Phys. Lett.* **94** 093304
[4] Liu Z, Oh J H, Roberts M E, Wei P, Paul B C, Okajima M, Nishi Y and Bao Z 2009 *Appl. Phys. Lett.* **94** 203301
[5] Oh M S, Hwang D K, Lee K, Im S and Yi S 2007 *Appl. Phys. Lett.* **90** 173511
[6] Li C S, Li Y N, Wu Y L, Ong B S and Loutfy R O 2008 *J. Phys. D: Appl. Phys.* **41** 125102
[7] Jo G, Hong W K, Maeng J, Choe M, Park W and Lee T 2009 *Appl. Phys. Lett.* **94** 173118
[8] Hwang D K, Oh M S, Lim J H and Park S J 2007 *J. Phys. D: Appl. Phys.* **40** R387–412
[9] Carcia P F, McLean R S and Reilly M H 2006 *Appl. Phys. Lett.* **88** 123509

[10] Oh B Y, Jeong M C, Ham M H and Myoung J M 2007 *Semicond. Sci. Technol.* **22** 608–12

[11] Frenzel H, Lajn A, Brandt M, Wenckstern H, Biehne G, Hochmuth H, Lorenz M and Grundmann M 2008 *Appl. Phys. Lett.* **92** 192108

[12] Jun J H, Park B, Cho K and Kim S 2009 *Nanotechnology* **20** 505201

[13] Yang C, Hong K, Jang J, Chung D S, An T K, Choi W S and Park C E 2009 *Nanotechnology* **20** 465201

[14] Shin K, Yang S Y, Yang C, Jeon H and Park C E 2007 *Appl. Phys. Lett.* **91** 023508

[15] Ohyama M, Kouzuka H and Yoko T 1997 *Thin Solid Films* **306** 78–85

[16] Lee C Y *et al* 2009 *Nanotechnology* **20** 425202

[17] Baruah S and Dutta J 2009 *Sci. Technol. Adv. Mater.* **10** 013001

[18] Yip G, Sugimoto S and Hattori R 2006 *J. Korean Phys. Soc.* **48** S102–6